Biochemistry

 Volume 41, Number 41 October 15, 2002

Accelerated Publications

The GAAA Tetraloop−Receptor Interaction Contributes Differentially to Folding Thermodynamics and Kinetics for the P4−P6 RNA Domain†

Brian T. Young and Scott K. Silverman*

Department of Chemistry, University of Illinois at Urbana-Champaign, 600 South Mathews Avenue, Urbana, Illinois 61801

Received July 21, 2002; Revised Manuscript Received August 29, 2002

ABSTRACT: Tetraloops with the generic sequence GNRA are commonly found in RNA secondary structure, and interactions of such tetraloops with "receptors" elsewhere in RNA play important roles in RNA structure and folding. However, the contributions of tetraloop−receptor interactions specifically to the kinetics of RNA tertiary folding, rather than the thermodynamics of maintaining tertiary structure once folded, have not been reported. Here we investigate the role of the key GAAA tetraloop−receptor motif in folding of the P4−P6 domain of the *Tetrahymena* group I intron RNA. Insertions of one or more nucleotides into the tetraloop significantly disrupt the thermodynamics of tertiary folding; single-nucleotide insertions shift the folding free energy by 2−4 kcal/mol ($\Delta\Delta G^{\circ\prime}$). The folding kinetics of several modified P4−P6 domains were determined by stopped-flow fluorescence spectroscopy, using an internally incorporated pyrene residue as the chromophore. In contrast to the thermodynamic results, the kinetics of Mg^{2+}-induced folding were barely affected by the tetraloop modifications, with a $\Delta\Delta G^{\ddagger}$ of 0.2−0.4 kcal/mol and a Φ value (ratio of the kinetic and thermodynamic contributions) of <0.1. These data indicate an early transition state for folding of P4−P6 with respect to forming the tetraloop−receptor contact, consistent with previous results for modifications elsewhere in P4−P6. We conclude that the GAAA tetraloop−receptor motif contributes little to the stabilization of the transition state for Mg^{2+}-induced P4−P6 folding. Rather, the tetraloop−receptor motif acts to clamp the RNA once folding has occurred. This is the first report to correlate the kinetic and thermodynamic contributions of an important RNA tertiary motif, the GNRA tetraloop−receptor. The results are related to possible models for the Mg^{2+}-induced folding of the P4−P6 RNA, including a model invoking rapid nonspecific electrostatic collapse.

The recent X-ray crystal and NMR structures of large folded RNAs have revealed a number of tertiary structure motifs (*1*). Prominent examples include relatively nonspecific interactions such as coaxial stacking of helices, as well as more specific interactions such as adenosine platforms, ribose zippers, base triples, and tetraloop−receptor motifs. Tetraloops are readily identified from sequence alignments (*2*), and they generally fall into several classes depending on sequence (the GNRA, UNCG, and CUUG tetraloops, where R is purine and N is any nucleotide) (*2*−*6*). The structures of isolated tetraloops have been extensively studied (*6*−*10*), and tertiary contacts between GNRA tetraloops and their receptors or other RNA elements have been demonstrated by biochemical experiments (*11*) and observed at high resolution (*12*, *13*). The GNRA tetraloop−receptor motif is robust enough to be used as the primary basis for engineering

† This research was supported by the Colgate-Palmolive Co. (Undergraduate Research Award to B.T.Y.), the Burroughs Wellcome Fund (New Investigator Award in the Basic Pharmacological Sciences to S.K.S.), and the University of Illinois Department of Chemistry.

* To whom correspondence should be addressed. Phone: (217) 244-4489. Fax: (217) 244-8024. E-mail: scott@scs.uiuc.edu.

10.1021/bi0264869 CCC: $22.00
Published on Web 09/17/2002

higher-order RNA assemblies (*14*, *15*), so it is clearly an important element of RNA tertiary structure.

All of the motifs mentioned above, including GRNA tetraloops with their receptors, have been identified in RNAs studied at their thermodynamic minimum, that is, in a stable folded state. The motifs are presumed to stabilize the folded state, and in some cases, the thermodynamic contributions of individual motifs have been quantified (ref *16* and references therein). However, RNA structure is dynamic (*17*), and RNA conformational changes clearly contribute to the catalytic properties of ribozymes, including the ribosome. What are the contributions of RNA tertiary structure motifs *during* the folding process itself, rather than after folding has ended?

We have examined this question for the GAAA tetraloop−receptor motif of the P4−P6 domain of the *Tetrahymena* group I intron RNA, a 160-nucleotide autonomous folding domain for which the structure and folding have been extensively studied (*12*, *16*, *18*−*22*). Previously, Abramovitz and Pyle modified the GAAA tetraloop that closes domain V of the yeast ai5γ group II intron RNA (*23*). They found that inserting one or more nucleotides between the second and third positions of the tetraloop (GA↓AA) led to measurable effects on the k_{cat}/K_m for splicing activity, but that the observed effects were more modest than might have been expected from perturbing a highly conserved structural motif. However, their system did not readily allow dissection of the kinetic versus thermodynamic basis for the effects of tetraloop modification, because their functional readout was catalysis and not folding. Here, we made similar modifications to the P4−P6 tetraloop and directly studied the thermodynamic effects on the fully folded state, as well as the kinetic effects on Mg^{2+}-induced folding. Our data reveal a striking difference between the thermodynamic and kinetic roles of the GAAA tetraloop−receptor motif in the Mg^{2+}-dependent folding of P4−P6. While the tetraloop−receptor motif contributes considerably to the thermodynamic stabilization of folded P4−P6, it participates very little during the rate-determining Mg^{2+}-induced folding step. These are some of the first data to focus specifically on understanding the role of a particular RNA tertiary structure motif during the folding process itself, rather than on the stabilization of the fully folded state.

MATERIALS AND METHODS

Cloning, RNA Preparation, and Radiolabeling. These were performed as described previously (*16*, *20*). A modified 15-mer RNA oligonucleotide with a U107-pyrene (pyr3) label was prepared by solid-phase synthesis (Dharmacon Research, Inc., Lafayette, CO), using the pyrene phosphoramidite reported earlier (*21*). The pyrene-labeled oligonucleotide was then attached by splint ligation as described previously (*21*) to T7 RNA polymerase transcripts comprising the remaining 145 nucleotides of P4−P6 plus any nucleotides inserted into the tetraloop.

Nondenaturing Gel Electrophoresis and Data Analysis. The Mg^{2+}-dependent nondenaturing gel electrophoresis (native PAGE)[1] experiments were performed as described

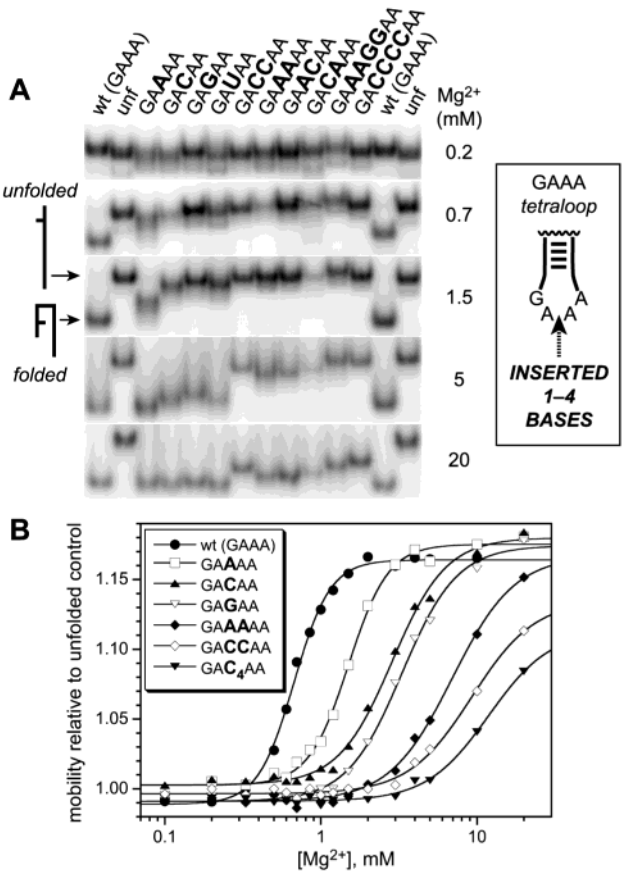

FIGURE 1: Nondenaturing PAGE for determining the thermodynamic perturbation ($\Delta\Delta G°'$) upon inserting nucleotides into the GAAA tetraloop of P4−P6. (A) Representative PhosphorImager data obtained at various Mg^{2+} concentrations [wt, wild-type P4−P6 RNA; unf, unfolded control mutant (*18*); the GAAA tetraloop sequence is shown with nucleotide insertions in boldface]. The location of the insertions in the L5b tetraloop of P4−P6 between positions A151 and A152 (*12*) is shown schematically on the right. (B) Plots of mobility vs $[Mg^{2+}]$, fit to a titration curve as described in Materials and Methods. Fit parameters and the calculated values of $\Delta\Delta G°'$ are given in Table 1.

previously (*16*), in 1× TB buffer [89 mM Tris and 89 mM boric acid (pH 8.3)] maintained at 35 °C. Values of $\Delta\Delta G°'$ for each modified RNA were calculated from the rightward shift in the Mg^{2+} midpoint for the mobility versus $[Mg^{2+}]$ curve as described previously (*16*), using the equation $\Delta G°' = nRT \ln[Mg^{2+}]_{1/2}$, where $[Mg^{2+}]_{1/2}$ is the Mg^{2+} concentration required to fold half of the molecules. An unresolved issue is whether $[Mg^{2+}]_{1/2}$ means "half of the molecules are fully folded and half fully unfolded" (i.e., two-state folding) or "on average, each molecule is half folded" (*24*); the data presented here do not address this question. Because $[Mg^{2+}]_{1/2,mod} > [Mg^{2+}]_{1/2,wt}$ for a destabilizing modification (i.e., the titration curve for a modified RNA is shifted to the right), $\Delta\Delta G°' > 0$ in such a case, and therefore, the data in Figure 1 show that all of the P4−P6 RNAs with modified tetraloops are thermodynamically destabilized relative to wild-type P4−P6. The Hill coefficient *n* for each modified RNA was assumed to be 4 for the purpose of calculating $\Delta G°'$ values from $[Mg^{2+}]_{1/2}$ values. For a complete discussion of this assumption, see ref *16*. If the Hill coefficient *n* for any particular modified RNA is actually less than 4 as observed for wild-type P4−P6, then the calculated $\Delta\Delta G°'$ for that modified RNA would be even larger than that

[1] Abbreviations: P4−P6, P4−P6 domain of the *Tetrahymena* group I intron RNA; P5abc, P5abc subdomain of P4−P6; PAGE, polyacrylamide gel electrophoresis.

Table 1: Thermodynamic Perturbations ($\Delta\Delta G^{\circ\prime}$) upon Modifying the GAAA Tetraloop of P4−P6[a]

tetraloop sequence	$[Mg^{2+}]_{1/2}$ (mM)	Hill coefficient *n*	$\Delta\Delta G^{\circ\prime}$ (kcal/mol)
GAAA (wild type)	0.68 ± 0.04	3.59 ± 0.27	(0)
GA**A**AA	1.50 ± 0.12	3.40 ± 0.26	2.0 ± 0.3
GA**C**AA	2.87 ± 0.52	2.51 ± 0.18	3.5 ± 0.5
GA**U**AA	2.93 ± 0.58	2.84 ± 0.20	3.6 ± 0.6
GA**G**AA	3.30 ± 0.58	2.46 ± 0.15	3.9 ± 0.5
GA**AA**AA	6.9 ± 3.0	2.16 ± 0.19	5.7 ± 1.4
GA**AC**AA	7.0 ± 3.6	2.23 ± 0.22	5.7 ± 1.8
GA**CA**AA	7.7 ± 4.3	2.37 ± 0.24	>6
GA**CC**AA	9.3 ± 5.3	2.14 ± 0.21	>6
GA**AAGG**AA	9.0 ± 5.5	2.33 ± 0.23	>6
GA**CCCC**AA	11.9 ± 10.4	2.19 ± 0.26	>6

[a] The nucleotide insertions (shown in boldface) are between A151 and A152 of the wild-type P4−P6 sequence (nucleotide numbering from ref *12*). Error ranges are the standard deviation for each $\Delta\Delta G^{\circ\prime}$ based on the fitting error and on the reproducibility between sets of experiments. The $[Mg^{2+}]_{1/2}$ values and Hill coefficients are from the specific experiment shown in Figure 1. As indicated in the text, the $\Delta\Delta G^{\circ\prime}$ values are calculated from the $[Mg^{2+}]_{1/2}$ values assuming $n = 4$. For $\Delta\Delta G^{\circ\prime}$ values of >6 kcal/mol, the assumption of a Hill coefficient of 4 introduces substantial uncertainty (*16*). For this reason and also because the $[Mg^{2+}]_{1/2}$ values themselves typically have a high level of error, more quantitative values of $\Delta\Delta G^{\circ\prime}$ are not estimated in these cases.

reported here (Table 1), which would further strengthen our conclusion about there being a difference between the thermodynamic and kinetic consequences of tetraloop modification.

Equilibrium Fluorescence Titrations with Mg^{2+}. The titrations were performed as described previously (*20*), in 1× TB buffer [89 mM Tris and 89 mM boric acid (pH 8.3)] at 35 °C on a ThermoSpectronic AB2 fluorescence spectrometer (λ_{exc} = 340 nm; relative fluorescence intensity monitored at 380 nm). For the equations used to fit the data, see ref *20*.

Stopped-Flow Fluorescence Spectroscopy. Stopped-flow fluorescence data were acquired on a ThermoSpectronic AB2 spectrometer equipped with a MilliFlow stopped-flow module. Samples of pyrene-labeled RNA (2−4 μM in 1× TB) and of $MgCl_2$ (20 or 200 mM in 1× TB) were equilibrated at 35 °C for >5 min before 1:1 mixing and data acquisition. The λ_{exc} was 319 nm; emission was collected at 380 nm (monochromator, 8 nm band-pass) and separately through a KV-370 cutoff filter (>370 nm). Both data sets typically gave similar results. Data were typically collected at 1.0 ms intervals out to 7 s. A total of 6−18 shots (typically 8) were averaged to provide the final data for fitting. Data acquired at 15 °C (not shown) were qualitatively similar to the data acquired at 35 °C (Figure 3).

RESULTS

Nondenaturing Gel Electrophoresis Reveals Thermodynamic Perturbations from Modifying the GAAA Tetraloop of P4−P6. Inspired by the study by Abramovitz and Pyle (*23*), we inserted one to four nucleotides into the GAAA tetraloop of P4−P6 as shown in Table 1 (a total of 10 modified RNAs, and the wild-type RNA). The thermodynamic consequences of these insertions were assayed by Mg^{2+}-dependent nondenaturing gel electrophoresis, which provides quantitative information about the contributions of structural motifs to P4−P6 folding (*16*). The basis of the assay is the differential electrophoretic mobility of folded and unfolded conformations of P4−P6, as described in more detail elsewhere (*16*) and shown schematically on the far left side of Figure 1A. Insertions into the GAAA tetraloop led to easily measurable rightward shifts in the mobility versus $[Mg^{2+}]$ curves (Figure 1B). Significantly, all of the single-nucleotide insertions led to curves that were shifted to the right but eventually rose to the same limiting relative mobility of ~1.15−1.20. Therefore, the overall structure of P4−P6 is retained approximately unchanged at high Mg^{2+} concentrations for these modified RNAs. The thermodynamic free energy perturbation $\Delta\Delta G^{\circ\prime}$ for each modified RNA was calculated from the magnitude of the rightward shift in the Mg^{2+} midpoint as described in Materials and Methods. The values of $\Delta\Delta G^{\circ\prime}$ are substantial, between 2 and 4 kcal/mol depending on the inserted single nucleotide (Table 1).

Insertion of more than one nucleotide had a larger effect. The mobility curves are still rising at the highest tested Mg^{2+} concentration of 20 mM, and the calculated values of $\Delta\Delta G^{\circ\prime}$ are at least 6 kcal/mol (Table 1). This is near the previously established upper limit for being able to quantify $\Delta\Delta G^{\circ\prime}$ values in this system (*16*). That is, the $\Delta\Delta G^{\circ\prime}$ values for these modified RNAs are best reported as being ≥6 kcal/mol, as in Table 1.

Equilibrium Fluorescence Spectroscopy Accurately Reports on the Thermodynamic Perturbations Due to Tetraloop Insertions. Because the nondenaturing gels necessarily examine the RNA at equilibrium, they are silent with regard to the kinetic contributions of the GAAA tetraloop that has been perturbed by modification. Previously, we documented that appending a pyrene chromophore onto the 2′-position of P4−P6 nucleotide U107 (near the 5′-terminal nucleotide G102) allows spectroscopic monitoring of the RNA's folded structure with millisecond time resolution, using the pyrene emission intensity as the signal (*20, 21*). Here, several of the tetraloop insertions were made in the U107-pyrene P4−P6 (see Materials and Methods) such that Mg^{2+}-induced stopped-flow fluorescence could be used to investigate the folding kinetics. First, the equilibrium fluorescence intensity as a function of Mg^{2+} concentration was examined, to verify that the fluorescence probe responded as expected to the thermodynamic perturbations. The same modifications that cause rightward shifts in the Mg^{2+}-dependent nondenaturing gel "titrations" (Figure 1) caused similar shifts in the fluorescence titrations (Figure 2; same rank order and approximate magnitude of shift for the various insertions; see the legend of Figure 2 for details). This demonstrates that the U107-pyrene fluorescence adequately reports on the tertiary structure of P4−P6 in the context of the tetraloop modifications.

Stopped-Flow Fluorescence Spectroscopy Reveals Very Small Kinetic Effects of the Modifications that Strongly Perturb the Thermodynamics of Folding. Having shown that the pyrene probe provides a reliable signal for the tetraloop-modified RNAs, we investigated their Mg^{2+}-induced stopped-flow folding kinetics. These experiments were performed at a final concentration after mixing of 10 mM Mg^{2+} (arrow in Figure 2). At this concentration, the portion of the fluorescence change due to tertiary folding is complete or nearly so (*20*), and the nondenaturing gel data also show that folding is complete, at least for the single-nucleotide insertions (Figure 1). Surprisingly, the single-nucleotide

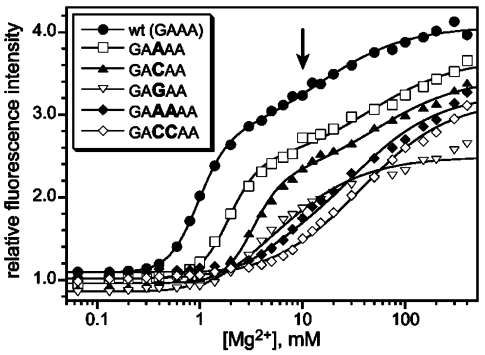

FIGURE 2: Equilibrium fluorescence titration with Mg^{2+} of pyrene-labeled RNAs with tetraloop modifications. Data are presented for modified RNAs in the same order as the plot of Figure 1B. Fits are to the equations of ref *20*, with the Hill coefficient *n* equal to 1 for the second (high-Mg^{2+}) transition. For the first three data sets (wt, GA**A**AA, and GA**C**AA), the Hill coefficient for the first transition equaled 3 (a higher value was not required to fit the data), and the $[Mg^{2+}]_{1/2}$ values were 0.97, 1.92, and 3.29 mM, respectively. The $\Delta\Delta G^{\circ\prime}$ values thus calculated assuming $n = 3$ are 1.3 (GA**A**AA) and 2.2 kcal/mol (GA**C**AA). These values compare reasonably well with those determined from nondenaturing gels (Figure 1), particularly considering the uncertainties in the Hill coefficients. For the remaining three data sets, the proximity of the presumed first and second transitions made curve fitting to multiple transitions difficult to believe; the fits shown are to single transitions. For each of the modified RNAs, note that qualitatively similar shifts in $[Mg^{2+}]_{1/2}$ were observed in both Figure 1 and this figure. For a more detailed discussion about the limitations of the fluorescence titration method and of the comparison between nondenaturing gel and fluorescence titration data, see ref *20*. The arrow indicates 10 mM Mg^{2+}, the concentration at which most of the stopped-flow data depicted in Figure 3 were recorded.

insertions that changed the folding free energy by 2−4 kcal/mol ($\Delta\Delta G^{\circ\prime}$) affected the folding rate by a factor of only ≤2 (Figure 3), which is equivalent to a free energy change $\Delta\Delta G^{\ddagger}$ of <0.5 kcal/mol at the folding transition state (Table 2). We also examined one double insertion (CC) at 100 mM Mg^{2+} (Figure 3; the higher Mg^{2+} concentration was required to observe reliably the fluorescence change upon mixing). Again, the substantial thermodynamic effect seen at equilibrium was not observed in the folding kinetics, as the folding rate dropped only 2-fold upon modification of the tetraloop.

The kinetic and thermodynamic data are correlated by plotting as shown in Figure 4. The slope of the fit line (Φ) equals $\Delta\Delta G^{\ddagger}/\Delta\Delta G^{\circ\prime}$. In the protein literature, such Φ value analysis has been used extensively to document the location of protein-folding transition states (*25*−*28*). A Φ value near 0 is deemed an "early" transition state, one that has adopted little if any of the structure found in the fully folded state. Conversely, a Φ of ≈1 is a "late" transition state in which folding is nearly complete. The slope of the fit line in Figure 4 is 0.07, clearly indicating an early transition state for P4−P6 folding with respect to forming the tetraloop−receptor interaction. That is, when folding is induced by mixing P4−P6 RNA with Mg^{2+}, the GAAA tetraloop−receptor motif forms its native structure only *after* the rate-determining folding transition state has been achieved.

DISCUSSION

The *Tetrahymena* group I intron P4−P6 domain has proven to be immensely useful for examining general principles of RNA structure and folding. This includes fundamental investigations of high-resolution RNA structure (*12*) and energetics (*16*), metal and water binding to RNA (*29*, *30*), and RNA folding mechanisms (*21*, *22*, *31*−*33*). Here, we sought to use P4−P6 as the model system for understanding the relationship between the thermodynamic and kinetic roles of an extremely common RNA tertiary structure motif, the GNRA tetraloop−receptor. Previously, interactions scattered throughout P4−P6 (including in the A-rich bulge and P5c stem) were examined for their thermodynamic and kinetic contributions (*22*), but no focused

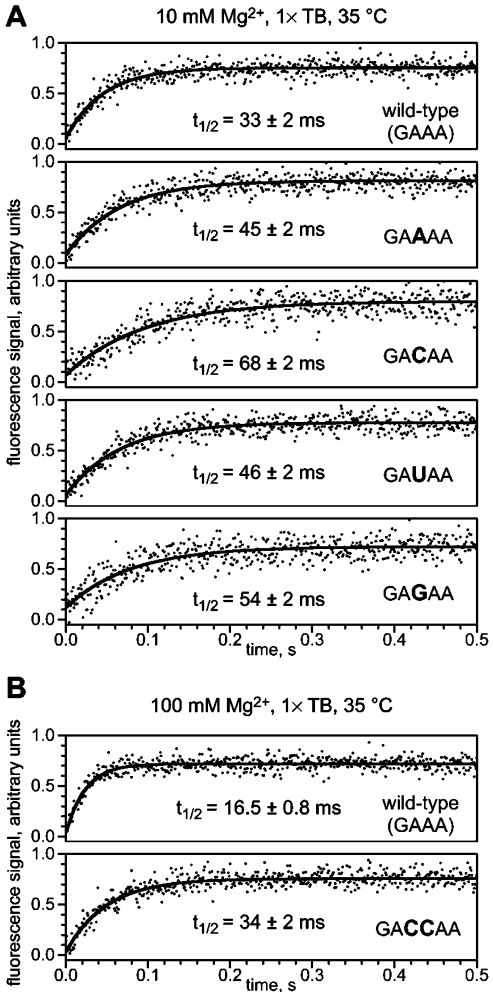

FIGURE 3: Stopped-flow fluorescence traces for Mg^{2+}-induced folding of U107-pyrene labeled P4−P6 domains. Data were collected in 1× TB at 35 °C; see Materials and Methods for details. The GAAA tetraloop sequence is shown with nucleotide insertions in boldface. (A) Data at a final Mg^{2+} concentration of 10 mM. (B) Data at a final Mg^{2+} concentration of 100 mM.

Table 2: Kinetic Parameters Observed upon Modifying the GAAA Tetraloop of P4−P6

tetraloop sequence	$[Mg^{2+}]$ (mM)	k_{obs} (s^{-1})	$t_{1/2}$ (ms)	$\Delta\Delta G^{\ddagger}$ (kcal/mol)[a]
GAAA (wild type)	10	21.2 ± 1.2	33 ± 2	(0)
GA**A**AA	10	15.3 ± 0.6	45 ± 2	0.19 ± 0.06
GA**U**AA	10	15.2 ± 0.6	46 ± 2	0.20 ± 0.06
GA**G**AA	10	12.8 ± 0.7	54 ± 2	0.30 ± 0.06
GA**C**AA	10	10.2 ± 0.4	68 ± 2	0.44 ± 0.06
GAAA (wild type)	100	42.1 ± 2.1	16.5 ± 0.8	(0)
GA**CC**AA	100	20.3 ± 0.8	34 ± 2	0.44 ± 0.05

[a] $\Delta\Delta G^{\ddagger} = RT \ln(k_{obs,modified}/k_{obs,wild-type})$ at 35 °C.

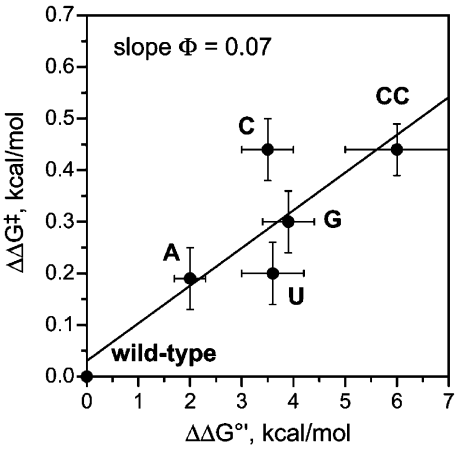

FIGURE 4: Correlating the kinetics and thermodynamics of folding for P4−P6 with modifications at the GAAA tetraloop. Data are taken from Table 1 (*x* values) and Table 2 (*y* values). The inserted nucleotides are labeled near each data point. Error bars are experimental errors from Tables 1 and 2. The weighted linear fit to all six data points has a slope of 0.07 (correlation coefficient $R^2 = 0.76$). The CC double insertion is included with a $\Delta\Delta G^{\circ\prime}$ of 6 ± 1 kcal/mol, although this value is uncertain as described in the text. If the CC data point is omitted, the linear fit appears to be similar, with a slope of 0.08 ($R^2 = 0.69$).

efforts were made on a specific structural motif such as the tetraloop−receptor, which is remote from the previously examined interactions.

A Sharp Distinction between the Effects of Tetraloop Modifications on the Thermodynamics and Kinetics of Formation of P4−P6 Structure. The data unambiguously reveal a striking contrast between the effects of GAAA tetraloop modifications on the thermodynamics and kinetics of tertiary structure formation in P4−P6. Modifications that significantly perturb the thermodynamics of folding of the entire RNA (Figures 1 and 2) barely affect the Mg^{2+}-induced folding transition state (Figure 3). The correlation of these observations in the context of Φ value analysis (Figure 4) provides a consistent picture in which the tetraloop−receptor interaction is largely unformed during the rate-determining folding step that is probed by U107-pyrene fluorescence. Because pyrene fluorescence tracks the overall folded state of the RNA at equilibrium (Figure 2 and ref *20*), we conclude that this tetraloop-independent rate-determining folding step involves global tertiary folding of the RNA. Thus, the tetraloop−receptor interaction does not direct the Mg^{2+}-induced folding of P4−P6, but instead acts to clamp the RNA closed once folding has ended. These data are the first to differentiate between the thermodynamic and kinetic contributions of a GNRA tetraloop−receptor motif to RNA folding.

The use of the "local" fluorescence probe U107-pyrene to monitor "global" P4−P6 RNA structure has been well-documented (*20*−*22*). It is important to note here that the stopped-flow kinetics are entirely (>95%) monophasic for each modified RNA that was examined, even for those with substantial ground-state thermodynamic perturbations due to insertion(s) into the tetraloop. This strongly suggests that a common folding transition is being observed for all P4−P6 variants, including those with even substantial thermodynamic perturbations, and that multiple folding pathways (*21*) are not complicating the observations.

Relationship of the Observations to Models of RNA Folding. The observations presented here may be considered in the context of two models for Mg^{2+}-induced P4−P6 RNA folding. Both this study and a previous report (*22*) conclude that modifications to various thermodynamically important regions of the P4−P6 RNA have surprisingly small kinetic consequences. In RNA folding model 1, these data suggest that we have yet to identify some key region of P4−P6 that directs its Mg^{2+}-induced tertiary folding. A candidate is the J5/5a "hinge" region (*24*), around which P4−P6 bends essentially in half upon binding Mg^{2+} (see the small cartoon images on the left side of Figure 1A). However, this model currently has no experimental support.

In alternative model 2, the available data collectively imply that *no region* of P4−P6 contributes to the Mg^{2+}-induced folding kinetics, and instead, the rate-determining folding step is dominated by nonspecific interactions. Recently, the general model of rapid, nonspecific electrostatic RNA collapse has received substantial experimental support (*34*−*36*). In this model, addition of Mg^{2+} induces a rapid yet nonspecific collapse of RNA to a compact structure in as little as several milliseconds, roughly analogous to forming a protein molten globule but with a different physical basis (*37*). On a longer time scale, perhaps minutes in the case of a large ribozyme, the RNA then adopts its fully native tertiary structure. Significantly, the studies that support this model were all performed with large multidomain RNAs, in which native structure requires both folding of individual domains and correct positioning of these domains relative to one another. No data have been published regarding collapse of an individual RNA domain such as P4−P6, where "domain" is used here according to the literature convention (*18*). The data reported here, in conjunction with those reported earlier (*22*), are consistent with this rapid nonspecific electrostatic collapse model for P4−P6 folding, although they do not prove the model.

Interactions involving the P5abc subdomain of P4−P6 and separately the GAAA tetraloop−receptor motif are generally considered to be the two main tertiary contacts enforcing the Mg^{2+}-dependent folded structure of P4−P6 (*19*). Because both of these regions have now been shown *not* to contribute to the folding kinetics (this report and ref *22*, respectively), and because no data positively identify regions of P4−P6 that would support model 1, we currently favor the nonspecific collapse model (model 2) for P4−P6 folding. However, the data are not conclusive either way, and at least two lines of future experimental inquiry may be fruitful. First, investigation of the J5/5a hinge region and other parts of P4−P6 should be undertaken to seek tertiary contributions to the folding kinetics. Second, it would be worthwhile to search experimentally for a collapsed intermediate for P4−P6 itself, in addition to large multidomain RNAs (*34*−*37*).

CONCLUSIONS

By a combination of nondenaturing gel electrophoresis and equilibrium and stopped-flow fluorescence spectroscopies, the GAAA tetraloop−receptor motif of the P4−P6 RNA domain has been shown to contribute much more strongly to Mg^{2+}-dependent thermodynamic stabilization of the folded state than to stabilization of the transition state for Mg^{2+}-induced folding. Thus, the main role of the tetraloop−receptor motif, at least in this RNA, is to maintain the RNA structure clamped in its folded state, not to direct

the folding process. These data are the first to distinguish the kinetic versus thermodynamic contributions of a very common RNA tertiary structure motif, the GNRA tetraloop−receptor. The results have been related to alternative models for Mg^{2+}-induced folding of the P4−P6 RNA domain, and they suggest specific experiments for discriminating between these models.

REFERENCES

1. Batey, R. T., Rambo, R. P., and Doudna, J. A. (1999) Tertiary Motifs in RNA Structure and Folding, *Angew. Chem., Int. Ed. 38*, 2326−2343.
2. Costa, M., and Michel, F. (1995) Frequent use of the same tertiary motif by self-folding RNAs, *EMBO J. 14*, 1276−1285.
3. Tuerk, C., Gauss, P., Thermes, C., Groebe, D. R., Gayle, M., Guild, N., Stormo, G., d'Aubenton-Carafa, Y., Uhlenbeck, O. C., Tinoco, I., Brody, E. N., and Gold, L. (1988) CUUCGG hairpins: extraordinarily stable RNA secondary structures associated with various biochemical processes, *Proc. Natl. Acad. Sci. U.S.A. 85*, 1364−1368.
4. Woese, C. R., Winker, S., and Gutell, R. R. (1990) Architecture of ribosomal RNA: constraints on the sequence of "tetra-loops", *Proc. Natl. Acad. Sci. U.S.A. 87*, 8467−8471.
5. Michel, F., and Westhof, E. (1990) Modelling of the three-dimensional architecture of group I catalytic introns based on comparative sequence analysis, *J. Mol. Biol. 216*, 585−610.
6. Jucker, F. M., Heus, H. A., Yip, P. F., Moors, E. H., and Pardi, A. (1996) A network of heterogeneous hydrogen bonds in GNRA tetraloops, *J. Mol. Biol. 264*, 968−980.
7. Heus, H. A., and Pardi, A. (1991) Structural Features That Give Rise to the Unusual Stability of RNA Hairpins Containing GNRA Loops, *Science 253*, 191−194.
8. Pley, H. W., Flaherty, K. M., and McKay, D. B. (1994) Three-dimensional structure of a hammerhead ribozyme, *Nature 372*, 68−74.
9. Scott, W. G., Murray, J. B., Arnold, J. R., Stoddard, B. L., and Klug, A. (1996) Capturing the structure of a catalytic RNA intermediate: the hammerhead ribozyme, *Science 274*, 2065−2069.
10. Correll, C. C., Munishkin, A., Chan, Y. L., Ren, Z., Wool, I. G., and Steitz, T. A. (1998) Crystal structure of the ribosomal RNA domain essential for binding elongation factors, *Proc. Natl. Acad. Sci. U.S.A. 95*, 13436−13441.
11. Jaeger, L., Michel, F., and Westhof, E. (1994) Involvement of a GNRA tetraloop in long-range RNA tertiary interactions, *J. Mol. Biol. 236*, 1271−1276.
12. Cate, J. H., Gooding, A. R., Podell, E., Zhou, K., Golden, B. L., Kundrot, C. E., Cech, T. R., and Doudna, J. A. (1996) Crystal Structure of a Group I Ribozyme Domain: Principles of RNA Packing, *Science 273*, 1678−1685.
13. Pley, H. W., Flaherty, K. M., and McKay, D. B. (1994) Model for an RNA tertiary interaction from the structure of an intermolecular complex between a GAAA tetraloop and an RNA helix, *Nature 372*, 111−113.
14. Jaeger, L., and Leontis, N. B. (2000) Tecto-RNA: One-Dimensional Self-Assembly through Tertiary Interactions, *Angew. Chem., Int. Ed. 39*, 2521−2524.
15. Jaeger, L., Westhof, E., and Leontis, N. B. (2001) TectoRNA: modular assembly units for the construction of RNA nano-objects, *Nucleic Acids Res. 29*, 455−463.
16. Silverman, S. K., and Cech, T. R. (1999) Energetics and Cooperativity of Tertiary Hydrogen Bonds in RNA Structure, *Biochemistry 38*, 8691−8702.
17. Cohen, S. B., and Cech, T. R. (1997) Dynamics of Thermal Motions within a Large Catalytic RNA Investigated by Cross-linking with Thiol-Disulfide Interchange, *J. Am. Chem. Soc. 119*, 6259−6268.
18. Murphy, F. L., and Cech, T. R. (1993) An Independently Folding Domain of RNA Tertiary Structure within the *Tetrahymena* Ribozyme, *Biochemistry 32*, 5291−5300.
19. Murphy, F. L., and Cech, T. R. (1994) GAAA Tetralooop and Conserved Bulge Stabilize Tertiary Structure of a Group I Intron Domain, *J. Mol. Biol. 236*, 49−63.
20. Silverman, S. K., and Cech, T. R. (1999) RNA Tertiary Folding Monitored by Fluorescence of Covalently Incorporated Pyrene, *Biochemistry 38*, 14224−14237.
21. Silverman, S. K., Deras, M. L., Woodson, S. A., Scaringe, S. A., and Cech, T. R. (2000) Multiple Folding Pathways for the P4−P6 RNA Domain, *Biochemistry 39*, 12465−12475.
22. Silverman, S. K., and Cech, T. R. (2001) An Early Transition State for Folding of the P4−P6 RNA Domain, *RNA 7*, 161−166.
23. Abramovitz, D. L., and Pyle, A. M. (1997) Remarkable morphological variability of a common RNA folding motif: the GNRA tetraloop-receptor interaction, *J. Mol. Biol. 266*, 493−506.
24. Szewczak, A. A., and Cech, T. R. (1997) An RNA internal loop acts as a hinge to facilitate ribozyme folding and catalysis, *RNA 3*, 838−849.
25. Fersht, A. R., Matouschek, A., and Serrano, L. (1992) The Folding of an Enzyme. I. Theory of Protein Engineering Analysis of Stability and Pathway of Protein Folding, *J. Mol. Biol. 224*, 771−782.
26. Serrano, L., Matouschek, A., and Fersht, A. R. (1992) The Folding of an Enzyme. III. Structure of the Transition State for Unfolding of Barnase Analysed by a Protein Engineering Procedure, *J. Mol. Biol. 224*, 805−818.
27. Fersht, A. R. (1995) Characterizing transition states in protein folding: an essential step in the puzzle, *Curr. Opin. Struct. Biol. 5*, 79−84.
28. Nymeyer, H., Socci, N. D., and Onuchic, J. N. (2000) Landscape approaches for determining the ensemble of folding transition states: Success and failure hinge on the degree of frustration, *Proc. Natl. Acad. Sci. U.S.A. 97*, 634−639.
29. Cate, J. H., and Doudna, J. A. (1996) Metal-binding sites in the major groove of a large ribozyme domain, *Structure 4*, 1221−1229.
30. Juneau, K., Podell, E., Harrington, D. J., and Cech, T. R. (2001) Structural Basis of the Enhanced Stability of a Mutant Ribozyme Domain and a Detailed View of RNA-Solvent Interactions, *Structure 9*, 221−231.
31. Doherty, E. A., and Doudna, J. A. (1997) The P4−P6 domain directs higher order folding of the *Tetrahymena* ribozyme core, *Biochemistry 36*, 3159−3169.
32. Doherty, E. A., Herschlag, D., and Doudna, J. A. (1999) Assembly of an exceptionally stable RNA tertiary interface in a group I ribozyme, *Biochemistry 38*, 2982−2990.
33. Deras, M. L., Brenowitz, M., Ralston, C. Y., Chance, M. R., and Woodson, S. A. (2000) Folding mechanism of the *Tetrahymena* ribozyme P4−P6 domain, *Biochemistry 39*, 10975−10985.
34. Russell, R., Millett, I. S., Doniach, S., and Herschlag, D. (2000) Small-angle X-ray scattering reveals a compact intermediate in RNA folding, *Nat. Struct. Biol. 7*, 367−370.
35. Buchmueller, K. L., Webb, A. E., Richardson, D. A., and Weeks, K. M. (2000) A collapsed non-native RNA folding state, *Nat. Struct. Biol. 7*, 362−366.
36. Webb, A. E., and Weeks, K. M. (2001) A collapsed state functions to self-chaperone RNA folding into a native ribonucleoprotein complex, *Nat. Struct. Biol. 8*, 135−140.
37. Russell, R., Millett, I. S., Tate, M. W., Kwok, L. W., Nakatani, B., Gruner, S. M., Mochrie, S. G., Pande, V., Doniach, S., Herschlag, D., and Pollack, L. (2002) Rapid compaction during RNA folding, *Proc. Natl. Acad. Sci. U.S.A. 99*, 4266−4271.

BI0264869